Diode Laser Spectroscopic Monitoring of Trace Gases

Frank K. Tittel
Rice University, Houston, USA

Konstantin P. Petrov
Gemfire Corporation, Palo Alto, USA

For references see page 1977

Modern diode laser spectroscopy is becoming an important and a more widely used tool for detection and measurement of trace gases. The change is driven by the recent advances in diode laser technology and diode laser frequency conversion techniques, which now push the limits of emission wavelength, output power, operating temperature, miniaturization, and cost. Basic features of the diode laser now find new, interesting, and unique use in well-established laboratory and field applications related to trace-gas detection, and in some instances even transform the traditional spectroscopic methods. It is the purpose of this chapter to familiarize the reader with the key elements of diode laser technology and analytical methods used in diode laser spectroscopy.

1 INTRODUCTION

Sensors based on tuneable diode lasers have found widespread applications to the sensitive and selective detection of environmentally important atmospheric trace gases in real time. The motivation for such precise species concentration measurements of gaseous compounds in ambient air includes such diverse fields as urban (e.g. automobile traffic, air quality in large enclosed structures), industrial (e.g. fence line perimeter monitoring in the petrochemical industry, combustion sites and waste incinerators), rural (e.g. horticultural greenhouses, rice agro-ecosystems) emission studies, chemical analysis and control for manufacturing processes (e.g. HF, NH_3 and HCl in semiconductor fabrication facilities and HF in aluminum smelters), biomedical sensing of physiologically important molecules (e.g. NO and CO), atmospheric chemistry (e.g. CO, CO_2, CH_4 and H_2CO in global studies of the environment), and spacecraft habitat air-quality monitoring.[1,2]

Numerous analytical instruments based on optical and nonoptical techniques have been developed in the past. In general, these instruments have some, but not all, of the desired characteristics that include: high sensitivity, selectivity, multicomponent detection capability, room temperature operation, large dynamic range, automatic operation, small size, high reliability, ease of use, and cost-effectiveness in terms of initial and maintenance costs. An ideal gas sensor technology that meets all these diverse requirements is, however, a challenging research and development task. Today's state-of-the-art laser spectroscopy, for example, is far from being able to meet these requirements, but recent significant technological advances may change the way it is used in future applications. Areas of technology that have seen a particularly strong improvement are tuneable diode lasers, both near-infrared (NIR) and mid-infrared (MIR); novel nonlinear materials for optical frequency conversion; optical fiber and semiconductor amplifiers; low-noise, room-temperature detectors; and advanced data acquisition and signal processing techniques.

Such new diode laser based spectroscopic sensors are beginning to provide excellent sensitivity and selectivity of an increasing number of organic and inorganic gaseous compounds in the infrared spectral region. This region consists of both the (NIR, 0.8 μm to 2 μm) that can be accessed by an increasing number of distributed feedback (DFB) telecommunications diode lasers and the (MIR, 2 μm to 20 μm) by lead-salt and antimony-based diode lasers, quantum cascade lasers, and compact sources based on difference-frequency mixing of commercially available diode and fiber lasers. Performance characteristics of several recent optical architectures of MIR gas sensors that have been developed and applied to real-world spectroscopic applications in the field and laboratory will be discussed. An effective method to increase sensitivity is to increase the effective optical path. This is possible for in situ, open path atmospheric measurements, but numerous applications require a compact extractive technique based on multipass cells (White, Herriott designs).

The NIR region is characterized by the presence of the first and second overtone and combination bands for many important gases. However, the transition strengths of the fundamental vibrational bands in the MIR are at least one to two orders of magnitude stronger, making this spectral regime the region of choice for high-sensitivity laser absorption spectroscopy. The detection sensitivity of current diode laser based gas sensors using direct absorption spectroscopy is limited by etalon fringes and laser feedback noise to 10^{-5} to 10^{-6} relative absorption. In addition to direct absorption spectroscopy, various techniques such as frequency modulation (FM), two-tone frequency modulation (TTFM) spectroscopy, balanced homodyne or balanced ratiometric detection (BRD) and cavity ring down spectroscopy (CRDS) can be utilized. Of these, only CRDS offers a means for avoiding the baseline variations caused by etalon fringes which often limit sensitivity.

2 FUNDAMENTALS OF GAS-PHASE SPECTROSCOPY

2.1 Atmospheric Trace Gases

Spectroscopic trace-gas detection is a method allowing one to compute concentration of a known gas, or

List of selected abbreviations appears in Volume 15

gases, from a measured optical absorption spectrum of the gas mixture (in practice, a small fragment of the spectrum may be measured). The procedure requires a good quantitative knowledge of the gas absorption characteristics. This knowledge is the realm of molecular spectroscopy, a complex and highly developed subject that is outside the scope of this chapter. A few fundamental spectroscopic concepts and formulae that are directly applicable to gas detection are, however, summarized in this section.

Each atom or molecule, small or large, is uniquely characterized by a set of energy levels. Transitions between levels by absorption or emission of electromagnetic radiation result in highly specific spectroscopic features. These features allow both the identification and quantification of the molecular species, such as atmospheric trace gases. Molecules may undergo transition between electronic, vibrational, and rotational states when exposed to electromagnetic radiation, resulting in absorption spectra. These spectra consist of a number of discrete absorption lines. Each line will have a certain linewidth and shape that depend on temperature and what surrounds the molecule, so the lines may form resolved or unresolved bands (see Figure 1); some will be intense while others will be weak. Transitions between molecular rotational–vibrational (ro-vibrational) states occur in the infrared "fingerprint" region of the electromagnetic spectrum, approximately between the wavelengths of 2.5 μm and 25 μm. Often also overtone and combination-overtone ro-vibrational bands are possible with significantly lower line intensity as compared to those for fundamental vibrational bands and the corresponding wavelengths are in the 0.8 μm to 2.5 μm spectral region. Transitions between electronic states of atoms and molecules occur in the ultraviolet and visible spectral region, 200 nm to 500 nm.

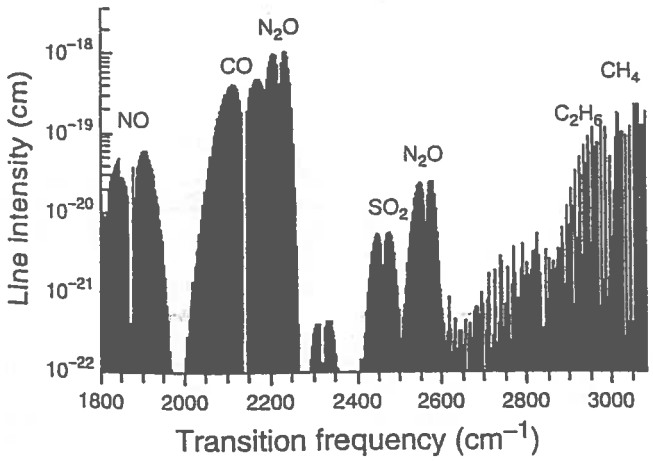

Figure 1 Survey absorption spectra of several atmospheric trace gases in the 3.1–5.6 μm wavelength region (3200–1800 cm^{-1}[3,4]).

All polyatomic molecules, with the exception of homonuclear diatomic molecules (e.g. N_2), absorb infrared radiation. The absorption changes the state of molecular rotation and vibration. An absorption spectrum therefore depends on the physical properties of the molecule such as size and shape and hence each molecule is characterized by a unique spectral "signature". Spectra of linear and some nonlinear polyatomic molecules consist of an array of individual or small groups of lines. In the case of large polyatomic molecules (e.g. benzene, C_6H_6) at atmospheric pressure, there are many lines overlapping each other, resulting in broad spectral features with some occasional peaks. These features occur in the majority of spectra and are the principal reason for the sensitivity and selectivity of trace-gas detection in the infrared.

There are numerous atmospheric trace gases (see Table 1). Their concentrations would normally be in the parts per billion (ppb, 10^{-9}) to parts per million (ppm, 10^{-6}) range. Minimum and maximum concentrations range from parts per trillion (ppt, 10^{-12}) to percent (%, 10^{-2}). There is much spectroscopic data available in the literature[1,2] and in electronic form which are important tools in the identification and development of specific detection strategies, especially in the presence of interfering species.[3–5]

Table 1 Analysis of atmospheric gas traces

Molecule	Absorption line (μm)	Overtone-MDC (ppm m)	Fundamental-MDC (ppm m)
CO_2	4.23	8[6]	0.0072
OCS	4.85	NA	0.023
N_2O	4.54	220[6]	0.036
	2.87		1.3
CO	4.6	100[7]	0.044
HCl	3.5	1.3[8]	0.050
HCN	3.0	0.29[9]	0.081
C_2H_6	3.34	NA	0.081
HF	2.4	0.2[10]	0.090
C_2H_2	3.08	0.08[9]	0.1
CH_4	3.3	15[8]	0.23
HBr	3.81	0.6[9]	0.32
H_2CO	3.6	50[9]	0.54
NO_2	3.46	0.5[11]	1.8
NH_3	2.94	2[12]	2.7
NO	5.3	60[9]	4
O_3	4.75	NA	9
SO_2	4.0	NA	40
H_2S	3.72	0.2[10]	54
H_2O	3.3	NA	NA

Values computed for the following parameters:
– Fundamental: $p = 100$ torr; $T = 298$ K; Min. detectable absorbance $= 2 \times 10^{-4}$ using direct absorption.
– Overtone: Min. detectable absorbance $\cong 1 \times 10^{-5}$ using either balanced detection/FM-techniques.
MDC, minimal detectable concentration.

For references see page 1977

2.2 Absorption Line Shape

In the absence of optical saturation and particulate-related scattering, the intensity of light $I(x)$ propagating in a homogeneous gas follows the Beer–Lambert law (Equation 1):

$$I(x) = I_0 \exp(-\sigma_m(\nu) N_m x) \tag{1}$$

Here m is the gas species index that labels the molecular concentration N_m and absorption cross-section $\sigma_m(\nu)$. The molecular absorption cross-section depends on frequency and has the units of cm^2 per molecule. It is the sum of cross-sections of all individual ro-vibrational transitions (Equation 2):

$$\sigma_m(\nu) = \sum_n S_n \Gamma(\nu - \nu_n) \tag{2}$$

We label the transitions using the index n; thus ν_n is the frequency of the n-th transition and S_n is its intensity. Technically both these quantities should also bear the index m to remind that they refer to a certain gas species, but for simplicity it is not done here.

The function $\Gamma(\nu)$ describes the line shape and has the same analytical form for all transitions. In MIR spectroscopy, the broadening of an individual transition due to finite upper-level lifetime is insignificant compared to broadening by the other two important mechanisms – thermal motion and molecular collisions. Their individual and combined effects on a molecular transition at a frequency ν_n are expressed as follows (Equations 3–7):

Thermal motion (Gaussian):

$$\Gamma(\nu) = \frac{1}{\Delta\nu_T \sqrt{\pi}} \exp\left[-\left(\frac{\nu}{\Delta\nu_T}\right)^2\right] \tag{3}$$

$$\Delta\nu_T = \frac{\nu_n}{c}\sqrt{\frac{2kT}{M}} \tag{4}$$

Molecular collisions (Lorentzian):

$$\Gamma(\nu) = \frac{1}{\pi\gamma_n P}\left[1 + \left(\frac{\nu}{\gamma_n P}\right)^2\right]^{-1} \tag{5}$$

Combined broadening (Voigt):

$$\Gamma(\nu) = \frac{1}{\gamma_n P} V\left(\frac{\nu}{\gamma_n P}; \frac{\Delta\nu_T}{\gamma_n P}\right) \tag{6}$$

$$V(x, y) = \frac{1}{\pi\sqrt{\pi}} \int_{-\infty}^{+\infty} \frac{\exp(-t^2)}{1 + (x + yt)^2}\, dt \tag{7}$$

Here c is the speed of light in vacuum, k the Boltzmann's constant, T the gas temperature, M the mass of the molecule, P the gas pressure, and γ_n the coefficient of pressure broadening. The quantities $\Delta\nu_T$ and $2\gamma_n P$ are referred to as the Doppler- and pressure-broadened linewidths. The line shape that results from the combined effect of Doppler- and pressure-broadening is a convolution of the two respective line shapes. It is known as the Voigt profile, and its mathematical expression $V(x, y)$ can not be further simplified. The physical significance of the convolution is that the Voigt profile has different asymptotic shapes for very low and very high gas pressure. At low pressure, molecular collisions are less frequent, leaving thermal motion the dominant broadening mechanism – the corresponding line shape is near-Gaussian. As the gas pressure increases the collisions take over, and the resulting line shape is near-Lorentzian (see Figure 2).

The previous expressions do not include the effect of pressure shift, which is typically in the range of several megahertz per atmosphere. The shift is very small compared to the width of an atmospheric-pressure-broadened line, typically several gigahertz.

It is common practice in infrared spectroscopy to express transition frequencies in inverse centimeters (cm^{-1}), or wavenumbers, defined simply as the inverse of the transition wavelength in vacuum, $\nu = \lambda^{-1}$. Multiplying this quantity by c gives the frequency in Hertz; thus 1 cm^{-1} is roughly 30 GHz. We shall use both units throughout this chapter, where appropriate.

One can verify, by integrating the absorption cross-section of an individual transition over frequency, that it is independent of the broadening mechanism and is equal to the line intensity S_n, in the units of cm per

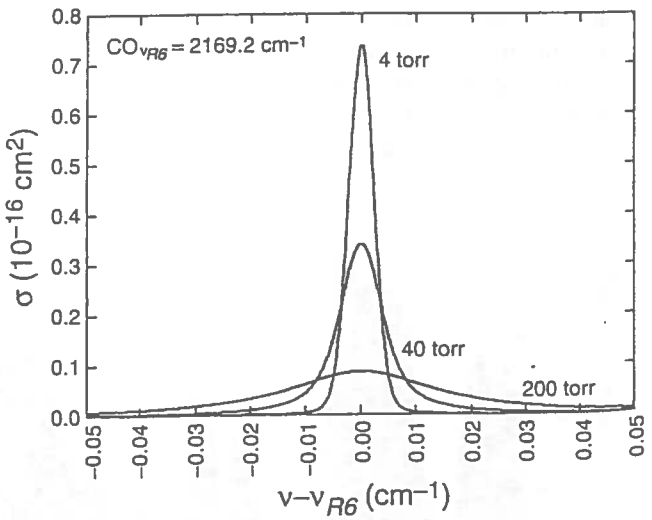

Figure 2 Frequency-dependent absorption cross-section of the R(6) fundamental transition of carbon monoxide at room temperature, plotted for different values of background air pressure. The horizontal axis is in cm^{-1} relative to the line center, $\nu_{R6} = 2169.2\,cm^{-1}$. Area under each curve, or line intensity, is the same: $S = 4.44 \times 10^{-19}$ cm. At 40 torr background air pressure, the Doppler- and collision-broadened linewidths are approximately equal: 0.003 cm^{-1}.

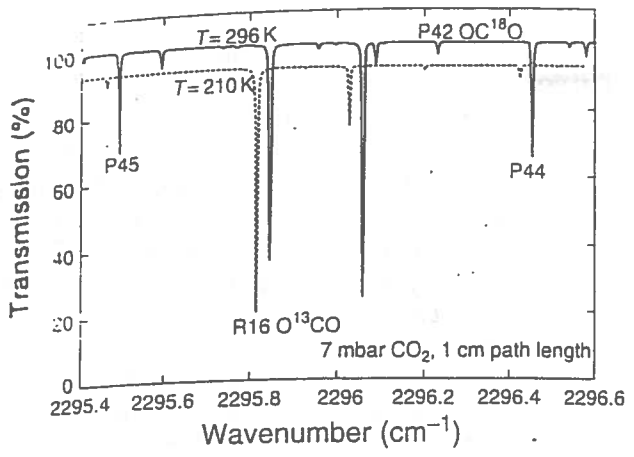

Figure 3 Absorption spectra of pure CO_2 at a pressure of 7 mbar over a 1 cm path calculated at two different temperatures using the HITRAN database.[4] The dotted trace has been offset for clarity and corresponds to $T = 210$ K, simulating the surface atmosphere of Mars. The strong dependence of line intensity on temperature for the transitions P44 and P45 should be noted.

molecule. Line intensity is proportional to the lower-state population density of a transition and thus depends on temperature (see Figure 3).

To a good approximation, especially at low temperatures, the sum of line intensities of all transitions in a band is independent of temperature and is known as the band strength B_m (Equation 8):

$$B_m = \int_{-\infty}^{+\infty} \sigma_m(\nu)\, d\nu = \sum_n S_n \tag{8}$$

It contains information on the vibrational electric dipole moment.[3] Thus in order to compute the absorption cross-section $\sigma_m(\nu)$ at any frequency, one must know the values ν_n, S_n, and γ_n for all transitions. These parameters have been measured and calculated for many lightweight gas molecules across the microwave and infrared spectrum, and compiled into extensive databases such as HITRAN[4] and GEISA.[5] Numerically accurate absorption spectra can be computed based on these data, not only for single gas species but for gas mixtures as well.

2.3 Spectra of Multicomponent Gas Mixtures

Analytical formulae given in the preceding section apply also to gas mixtures. The total absorption cross-section $\sigma(\nu)$ is then a weighted average of absorption cross-sections of individual species, with the mole fraction C_m of each species used as the weight coefficient (Equations 9 and 10):

$$\sigma(\nu) = \sum_m C_m \sigma_m(\nu) \tag{9}$$

$$\sum_m C_m = 1 \tag{10}$$

For each of the m species, the pressure broadening coefficients γ_n generally depend on the transition. They also depend on the type of molecule with which the collisions occur. In general, partial pressures in conjunction with the appropriate pressure-broadening coefficients should be used to compute the overall pressure broadening from all gases present in the background (this includes self-broadening). Air-broadening coefficients are particularly useful in calculations, and are listed in spectroscopic databases.[4,5]

In trace-gas sensing applications, however, the species of interest are often present in very low concentrations, so that self-broadening and broadening against other trace gases can be neglected in calculations, and air-broadening alone will suffice. For the conditions of atmospheric pressure broadening, $\gamma P \gg \Delta\nu_T$, the Doppler contribution to the overall linewidth can often be neglected, and the line shape be treated as pure Lorentzian. Likewise, at pressures low enough to ensure $\gamma P \ll \Delta\nu_T$, the line shape can be treated as pure Gaussian. In either case, calculation of the line profile is simplified considerably.

At intermediate total pressures, $\gamma P \sim \Delta\nu_T$, which for most lightweight gases range from 5 to 100 torr, calculation of the Voigt profile is necessary to obtain numerically accurate absorption spectra. Methods for approximate calculation of the Voigt profile, and the related plasma dispersion function, are now a well-developed subject. We have found the approximations published by Humlicek[13] to be particularly useful.

3 LASER SPECTROSCOPIC SOURCES

3.1 Advantages of Diode Lasers

Soon after the first semiconductor (diode) laser was developed in 1962, diode laser spectroscopy became a firmly entrenched technique for detection, identification, and measurement of molecular and atomic species in the gas phase. The reason for its wide acceptance in the scientific community was twofold. First, narrow-linewidth light sources such as lasers were well suited for probing the inherently narrow molecular and atomic transitions, so that both the line shape and intensity could be measured accurately and rapidly. Lasers simply offered better wavelength resolution (linewidth) and spectral brightness (power emitted per unit linewidth) than conventional grating or prism monochromators. Second, among all lasers, diode lasers offered a unique combination of tuneability, output power, small size, and modulation capabilities (see Table 2). In other words they are significantly more convenient to use than other sources. Perhaps the most important advantages of diode lasers are the simple excitation in the form of electric

For references see page 1977

Table 2 Performance characteristics of room-temperature single-frequency diode lasers

Parameter	Unit	Typical values
Center wavelength	nm	670, 780, 810, 860, 980, 1060, 1310, 1550
Gain bandwidth	nm	20–50
Output power	mW	3–200
Mode size	μm	1 × 3
Linewidth	MHz	10–300
Tuning response	nm/K	0.1–0.3
Tuning response	GHz/mA	0.3–2
Threshold current	mA	20–90
Modulation bandwidth	GHz	2–40

current and the fact that the laser wavelength and output power depend on the current. For small changes in the injection current, that dependence is nearly *linear* and *instantaneous*, allowing predictable and fast wavelength control. This advantage is discussed in section 4.3.

Diode laser spectroscopy is divided into two categories according to the spectral region used. MIR spectroscopy is used in the "fingerprint" region from 2.5 μm to 25 μm where most molecular species exhibit fundamental absorption. It offers the highest detection sensitivity among spectroscopic methods, primarily because the fundamental absorption bands are very strong. Diode lasers operating at MIR wavelengths typically deliver 100-μW output power and require cryogenic cooling (more on this in section 3.3). NIR, or "overtone", spectroscopy employs room-temperature diode lasers at wavelengths below 2 μm. Detected here are the short-wavelength molecular overtone transitions that are typically a factor of 30 to 300 weaker than the fundamental transitions. The two types of molecular spectroscopy just described represent the two different choices made in the tradeoff between absorption strength and the optical power available to detect it. MIR spectroscopy is used whenever higher sensitivity is needed, but at the expense of cryogenic cooling. Overtone spectroscopy is the method of choice in applications where lower sensitivity can be tolerated, but where low cost, reliability, and room-temperature operation are paramount. Alternative techniques for the generation of MIR light for spectroscopic applications will be discussed in section 3.4.

3.2 Overtone Band Detection with Near-infrared Diode Lasers

NIR spectrometers usually employ commercial diode lasers with emission wavelengths from 780 nm to 1900 nm. Gas detection at these wavelengths is based on the molecular vibration overtone and combination-overtone bands that are significantly less intense than the fundamental bands. For example, the lines of the first overtone stretch vibration band of methane centered at 1.6 μm is roughly 160 times weaker than the fundamental band. Thus ambient methane would cause a 0.005% absorption over a 1-m path length at this wavelength at room temperature.[4] Reliable measurement of such low absorption is difficult even under laboratory conditions, so longer path lengths or special measurement techniques are necessary to render a satisfactory signal-to-noise ratio for applications requiring trace-level monitoring.

Overtone spectrometers usually have plenty of optical probe power to deal with this problem. NIR diode lasers emit anywhere from 1 to 100 mW of single-frequency radiation with low excess noise: 15 to 35 dB over shot noise limit is typical, and it can be detected with a silicon photo-diode.[14] They are fast, with modulation bandwidths of over a gigahertz allowing rapid scanning, fast FM, and leading to gas detection in real time.

High output power levels have two important benefits. First, detector noise can be neglected and the measurement of absorption be performed near the optical shot-noise limit. For example, Allen et al.[15] report a detection sensitivity of $2 \times 10^{-7}\,\mathrm{Hz}^{-1/2}$ absorption units with the use of a 1.3-μm diode laser and a balanced ratiometric detector. Second, with high initial power available in a beam, one can employ a multi-pass cell to propagate the beam back and forth through a gas sample, achieving long effective path lengths and thus increasing the observed absorption signal. Although the throughput of such a cell decreases exponentially as the number of passes increases (also see section 4.1), there is still plenty of light left at the end to permit measurements that are not limited by detector noise.

NIR overtone spectrometers, such as one developed by Uehara and Tai,[16] are usually built to detect one or a few specific gases, for two reasons. First, the NIR wavelength region from 780 to 1900 nm is not covered completely; diode lasers are available at only few discrete wavelengths, and each has a limited tuning range when operated without an external cavity. Second, these devices are relatively inexpensive – sometimes under $50 in small quantities – making it economical to have several dedicated lasers, each detecting one gas species, in a single instrument. This configuration is also attractive because different gas species can be measured in parallel. For example, several groups have developed a gas sensor that can do this using one common beam path through the sample and one detector.[17]

Alternatively, a single external-cavity diode laser (ECDL) with a large tuning range can be used. In an ECDL, one or both faces of the laser chip are anti-reflection-coated to eliminate optical feedback. The feedback is provided by a larger, external cavity. The cavity acts as a wavelength selector, picking a specific

wavelength out of the usually broad gain spectrum of the semiconductor laser material. Several cavity configurations have been developed that differ in the method of tuning, component count, output beam characteristics, and output coupling efficiency. Figure 4 shows a frequently used external cavity type, known as the Littman configuration. It employs a diffraction grating as a wavelength discriminator. The first-order diffracted beam is folded back into the cavity by a mirror that acts as a tuning element – its angle and position determine the output wavelength. The grating also functions as an output coupler, producing the zero-order (reflected) beam whose angle and point of origin are independent of wavelength. Mode-hop-free single frequency tuning ranges of over 1000 GHz have been demonstrated for an ECDL.[18] A spectrometer based on such a widely tuneable laser is a very useful tool in that it can acquire spectra of an entire molecular band in a single electronically controlled scan in a matter of seconds. Oh and Hovde,[19] for example, used a widely tuneable 1.5-μm ECDL to record a spectrum of the $\nu_1 + \nu_3$ stretch-vibration combination band of acetylene.

NIR diode lasers often come in compact sealed packages that include a convenient fiber-coupled output. Thus the probe light can be delivered from a single source to several sampling locations. Likewise, the radiation passing through the sample can be returned to a detector via a fiber, sometimes even the *same* fiber (see Figure 5).

A general problem that is faced is interference by water vapor. Long path lengths do not help here as they increase not only the signal of interest but the interfering absorption as well. Multicomponent spectral

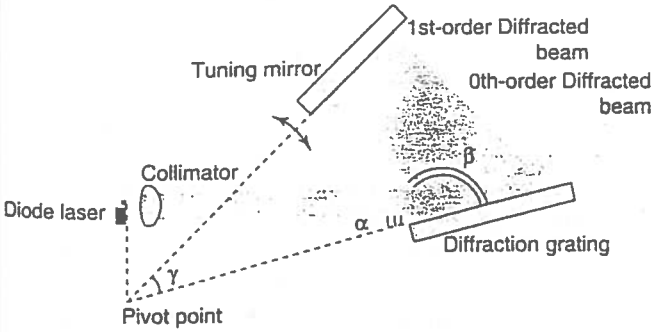

Figure 4 Optical diagram of an ECDL. Light at a wavelength λ emitted by the laser chip is collimated and is incident upon a diffraction grating with a period b. The first-order diffracted beam emerges at an angle to the grating, such that $\cos\alpha - \cos\beta = \lambda/b$, and is folded back into the cavity by an adjustable mirror. The round-trip distance traveled by light in the cavity must be an integer number of wavelengths. Continuous wavelength tuning results when both these conditions are met; this is accomplished by rotation of the tuning mirror around a pivot point located outside the laser cavity as shown.

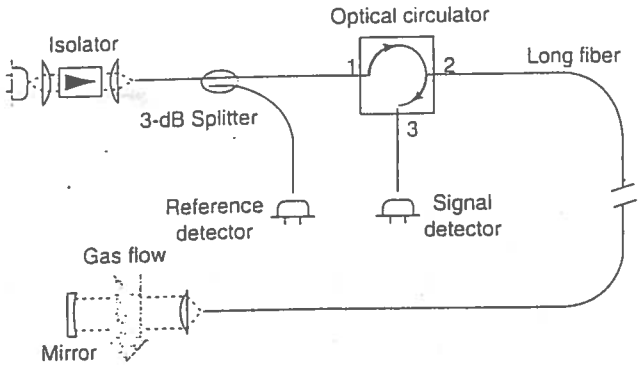

Figure 5 Schematic of a NIR diode laser spectrometer using a single fiber to deliver the light to and from the sampling location. The reference detector monitors the laser output power during frequency scans. The optical circulator transmits light from port 1 to 2 and from 2 to 3. and is used to route the returned beam to the signal detector.

fitting algorithms have been developed that can resolve weak absorption lines of interest in the presence of heavy interference by a known gas. The problem becomes far more severe, however, when the identity of the interfering species is unknown.

3.3 Fundamental Band Detection with Lead-salt Diode Lasers

Lead-salt diode lasers have been developed for operation at wavelengths from 3 to 30 μm. They typically deliver 10–500 μW of output power in a near-diffraction-limited beam and can be tuned by temperature or current control. These lasers are based on PbS, PbSe, or PbTe semiconductors and generally require cooling near the temperature of liquid nitrogen, although recently a continuous wave (CW) operation has been achieved at temperatures as high as 195 K.[20]

MIR spectrometers employing lead-salt diode lasers have shown perhaps the most impressive performance to date in terms of minimum detectable gas concentration. There are four reasons for this. First is the very high absorption strength of the fundamental molecular vibrational bands. For example, carbon dioxide at a 3.3 ppm concentration in air (which is roughly 100 times lower than its typical ambient level) will cause absorption of 15% at 4.23 μm over a 1 m path. Such macroscopic absorption signals can be easily measured even without sophisticated signal processing techniques. Second, lead-salt diode laser spectrometers use cryogenically cooled InSb or HgCdTe detectors with noise-equivalent powers in the range of 0.5 to 50 pW $Hz^{-1/2}$, and although the lead-salt lasers produce less output power than their NIR counterparts, there is still enough light to render the detector noise virtually nonexistent and allow shot-noise-limited detection. Third, near-diffraction-limited

For references see page 1977

beam characteristics of lead-salt diode lasers allow beam shaping and propagation over long distances: this makes it possible to use multipass cells or remote sampling in open air. Fourth, lead-salt diode lasers have FM capabilities similar to those of NIR diode lasers, allowing the use of harmonic detection and two-tone modulation techniques – efficient methods of noise bandwidth reduction, to be discussed in section 4.3.

These advantages add up to a real-world instrument performance that is impressive.[21] Schiff et al.[22] report the detection limit 75 ppt for airborne measurements of HNO_3 in the continental boundary layer with a response time of 3 minutes. Werle and company[23] achieved a detection limit of 10 ppt for NO_2 under laboratory conditions using a signal averaging time of 25 s.

Although well entrenched in a spectroscopic laboratory, lead-salt diode lasers are seldom used in industrial applications. Preventing their wide acceptance are several important practical drawbacks. Perhaps the most serious one is the large manufacturing spread of operating wavelengths. The situation is aggravated by the fact that each individual laser has a rather limited tuning range, typically 100 cm^{-1} with temperature control, and that the range itself is not free of mode hops. This makes it difficult to find a laser chip that actually tunes to a specific wavelength – a situation potentially catastrophic in applications where there is a limited choice of absorption lines free from interference by other lines, e.g. detection of formaldehyde.[24]

A more subtle problem with lead-salt diode lasers has to do with thermal cycling, a process in which a laser is simply warmed up to room temperature and then cooled back to its normal operating temperature. The simple process tends to cause irreversible changes in prior laser tuning characteristics and emission wavelength.

Despite these and other technical difficulties, several specialized trace-gas sensors based on lead-salt diode lasers have been developed for field use. These instruments show excellent performance, proving just how effective the use of a MIR diode laser can be. For example, Webster et al.[25] reported the design and operation of a fully automatic, compact sensor for the measurement of five trace gases in the lower stratosphere on board an airplane. Their instrument houses four lasers and four detectors mounted on the same liquid-nitrogen-cooled platform, beam shaping optics, a compact multipass absorption cell with 80 m path length, analog electronics, and a computer-controlled data storage system. It is capable of detecting optical absorption as small as 10^{-5} which corresponds to detection limits in the range of several tens of ppt for species such as HCl, NO_2, HNO_3, CH_4, and N_2O. Podolske and Loewenstein[26] report construction and performance of a similar instrument that uses an additional, "zero", beam for removing the background absorption signal caused by gases within the instrument case. Both instruments employ wavelength modulation (WM) and second harmonic detection to achieve high sensitivity.

3.4 Diode Laser Frequency Conversion

A more recent technique for producing spectroscopic MIR light is laser difference-frequency generation (DFG). Two laser beams at different frequencies combined in a nonlinear material with suitable dispersion characteristics can generate a beam at the difference-frequency ("idler"). Narrow emission spectra of the two lasers, usually referred to as "pump" and "signal", translate into a similarly narrow spectrum of the idler wave. Idler wavelength tuning is accomplished by tuning of the pump laser, or signal laser, or both (see Figure 6).

In the early demonstration of this method by Pine,[27] an argon-ion laser output and a dye laser output were combined in bulk lithium niobate to produce a narrowband (15 MHz), 2.2–4.2 μm tuneable radiation. However, NIR diode lasers can now be used instead,[28] making it feasible to construct compact MIR spectrometers that operate at room temperature (see Figure 7). Thus the convenience and practicality of NIR diode laser technology are combined with analytical power of MIR spectroscopy in a single instrument. Such an instrument inherits the single-frequency operation and high speed modulation capabilities of diode lasers, and takes advantage of their relatively wide tuning range. For example, a typical 780-nm diode laser (see Table 2) can be tuned over 20 nm, or 2.6% in wavelength, by temperature control without appreciable change in output power. When the output of such a laser is down-converted by mixing with a 980 nm diode laser, the tuning range in frequency units remains the same, in this case a very significant tuning range: 3.6–4.1 μm, or 13% in wavelength.

The practicality of diode-pumped MIR frequency conversion received a significant boost from the development of novel nonlinear materials, such as periodically poled lithium niobate ($LiNbO_3$), lithium tantalate ($LiTaO_3$), and potassium titanyl phosphate ($KTiOPO_4$, or KTP) at wavelengths in the 2.5–5.2 μm spectral region.[29] Quasi-phase matching properties of each of these crystals can be engineered for interaction of any pump and signal wavelengths within transparency range of the crystal, allowing significant flexibility in the choice of laser sources.[30]

Although routinely used for spectroscopy and gas detection, the DFG in bulk nonlinear crystals is characterized by low conversion efficiency, typically in the range of 0.002–0.05% W^{-1} cm^{-1}.[31] A detailed quantitative theory of this nonlinear optical process, developed by Boyd and Kleinman,[32,33] is beyond the scope of this

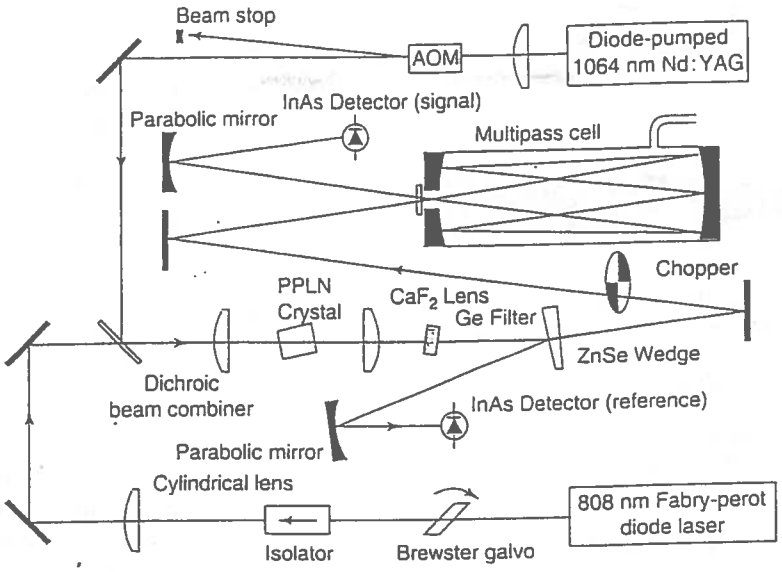

Figure 6 Schematic of difference-frequency spectrometer. A free-running Fabry–Perot diode laser at 808 nm, the "pump", is mixed with a diode-pumped Nd:YAG laser, the "signal", in a periodically poled $LiNbO_3$ (PPLN) crystal to produce a 3.4-μm tuneable radiation. An antireflection-coated germanium filter blocks the residual pump and signal light.[44]

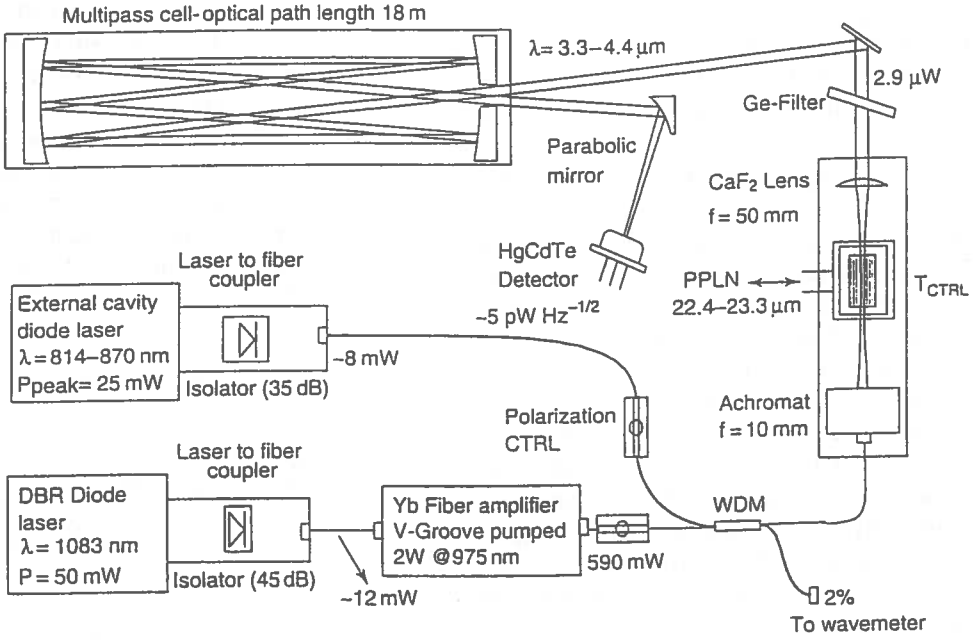

Figure 7 Portable diode-pumped difference-frequency spectrometer for detection of trace gases.[69] DBR: distributed Bragg reflector.

review chapter, so we will state simply that the maximum idler power generated in a given crystal is proportional to the product of crystal length, pump power, signal power, and the squared second-order nonlinear coefficient of the crystal. Maximum DFG output power is achieved by means of optimal focusing,[34] for which any further increase in beam intensity through tighter focusing is offset by a decrease in interaction length due to diffraction, resulting in no gain in output power. For DFG radiation longer than 5 μm it is possible to use birefringent bulk nonlinear optical materials, such as $AgGaS_2$, $AgGaSe_2$, GaSe and in the future, quasi-phase matched GaAs.

The tradeoff between beam size and interaction length can be eliminated altogether in guided-wave DFG. Tight optical confinement of pump and signal radiation near the waveguide core creates a region of high intensity and good

For references see page 1977

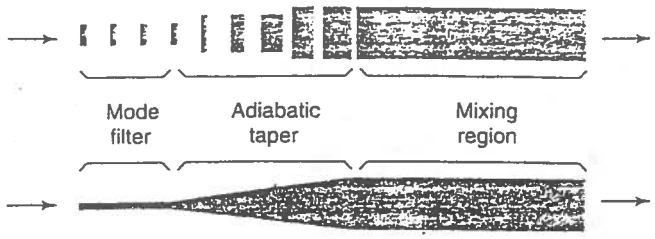

Figure 8 Alternative geometries of a tapered waveguide for difference-frequency mixing. Shaded regions indicate material with higher index of refraction. Laser light is launched into the mode filter that carries a single (fundamental) spatial mode. The mode size is then adiabatically converted to fit the mixing waveguide which is multimode. Periodic segmentation[38,39] of the waveguide acts to reduce the effective index. It also provides independent control of the effective waveguide width and depth.

modal overlap which are both maintained throughout, and independent of, the length of the waveguide.[35] Interaction length is now limited by the length of the waveguide, not diffraction. Guided-wave parametric processes, such as OPO, SHG, and DFG, have been demonstrated in periodically poled $LiNbO_3$, $LiTaO_3$, and KTP. In $LiNbO_3$, for example, a waveguide can be formed by titanium in-diffusion,[36] or a $^+Li \longleftrightarrow {}^+H$ ion exchange.[37] The latter process is normally followed by several hours of annealing at elevated temperature to create a graded index distribution.

A DFG waveguide designed to carry a single spatial mode at the idler wavelength is necessarily multimode at the shorter, pump and signal wavelengths. The presence of multiple spatial modes complicates the waveguide phase matching characteristics considerably. For example, a TM_{00} (fundamental) mode at the signal wavelength will interact with TM_{02} and TM_{10} modes at the pump wavelength, but not with TM_{01} or TM_{11} modes. Efficient and reproducible fundamental-mode excitation of a DFG waveguide was first achieved by Chou et al.,[38] who used a combination of a mode filter and an adiabatic taper (see Figure 8). An improved device featuring separate inputs for the pump and signal beams followed by a directional coupler has also been demonstrated.[39] DFG waveguides have been used to build viable sources of MIR radiation for spectroscopic purposes.[46]

4 TECHNIQUES FOR THE MEASUREMENT OF SMALL GAS CONCENTRATIONS

4.1 Long Path Length and Cavity-enhanced Spectroscopy

Gas sensors often deal with gas concentration and sample size so small that the detected full-scale absorption signal is indistinguishable from system noise. This is no surprise, since most photons in the probe beam pass through the sample without being absorbed. If one were able to somehow "recycle" these unabsorbed photons, by forcing them to pass through the sample many times, one would obtain better contrast between signals on and off resonance of the molecular transition. Two different forms of this idea have been developed to date.

Long-path length spectroscopy, not to be confused with remote sensing or fence-line monitoring,[41] refers to the use of an optical set-up that provides multiple passes of the probe beam through a relatively small sample volume. An example is the Herriott cell, a device with two identical spherical mirrors facing each other and separated by nearly their radius of curvature (see Figure 9). A probe beam launched through a hole in one of the mirrors at an angle to the optical axis, completes a certain number of passes between the mirrors, and exits through the same hole. The mirror curvature, applied to the beam at each reflection, keeps it from diverging, as if in a cavity. The beam bounce pattern and path length can be controlled by adjusting the mirror separation. The picture is deceptively simple, but certain design rules must be followed to ensure that the beam exit the cell after a controlled number of passes, especially in the case of astigmatic mirrors.[42] The number of passes can routinely exceed 100, thus providing a commensurate improvement in signal strength (see Figure 10). It is important to recognize that mirrors are not perfect, and a small portion of the probe light is lost to absorption and scattering each time the beam bounces. Optical throughput of the cell thus decreases exponentially with the number of passes, whereas the

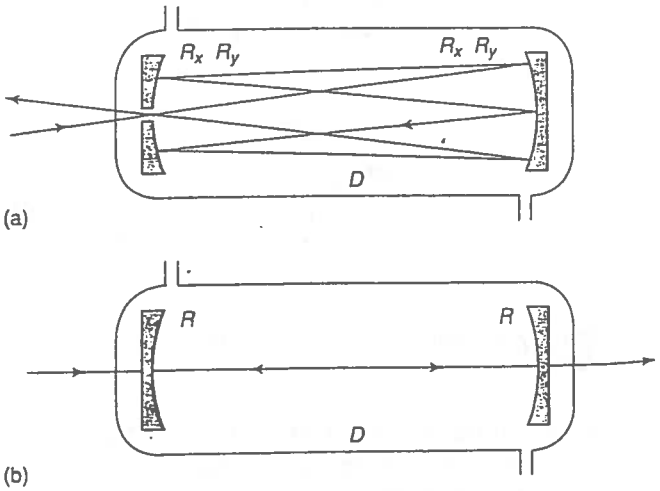

Figure 9 Schematic of a multipass cell (a). The standard Herriott cell has two spherical mirrors separated by nearly their radius of curvature $D \approx R_x = R_y$. Unlike with the confocal cavity (b), a resonance does not occur in the multipass cell because the beam never hits the same spot twice on any mirror before it exits through the coupling hole.

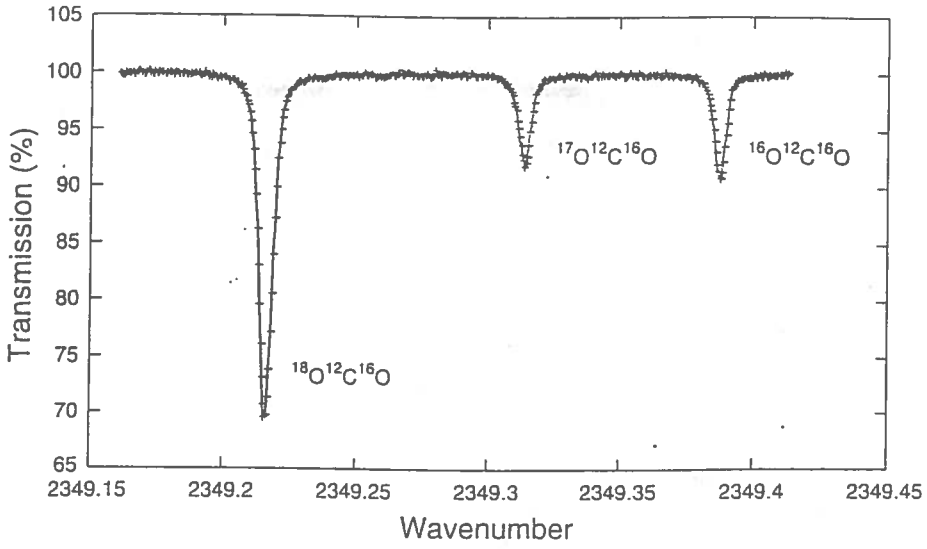

Figure 10 Direct-absorption spectrum of three different isotopes of natural CO_2 in air at a pressure of 3.6 kPa in an 18-m multipass cell. The probe beam makes 90 passes between the cell mirrors that are 20 cm apart. Given the cell transmission of 33%, the overall gain in signal strength is 30.[65] Interference fringes, due to light scattered by the mirrors, can be seen in the baseline.

detected peak-to-peak absorption only increases linearly (in the small-signal limit) with the number of passes.

Several configurations of the multipass cell are available that offer different mirror counts, input and output ports, and beam patterns. They can be sealed, for the measurement in static gas samples or controlled gas flows, or open to ambient air. Performance of long path length multipass cells, especially those with dense beam patterns, suffers from optical interference ("fringes") due to light scattering by the cell mirrors. The fringe magnitude is sensitive to optical alignment and is typically on the order of 0.01–0.1% full-scale transmission (see Figure 10). Mirror drift and vibration can also become a problem, as they modulate the cell transmission. Mirror vibration, on the other hand, reduces the effective magnitude of interference fringes, as it scrambles the phase of optical feedback within the cell.

Cavity-enhanced spectroscopy is another method to increase the magnitude of absorption signal when only a small gas sample is available. Although its implementation and treatment are different from those described above for the multipass cell, the similarity is evident if one considers the idea of "recycling" photons in the probe beam. In this method, a weakly absorbing gas sample is placed inside a cavity, and the cavity is tuned to resonance with the probe beam, e.g. by a piezo-driven cavity mirror. At the peak of resonance, the cavity photon lifetime significantly exceeds the cavity round-trip time, thus increasing the probability of interaction with gas molecules in the sample. The effective number of passes between cavity mirrors, N, constitutes the improvement in the magnitude of absorption signal and is proportional to cavity finesse, F, which can be made rather high Equation (11):[43]

$$N = 2\frac{F}{\pi} \tag{11}$$

This approximation is good for weak absorption signals. A point to consider here is that increased gas absorption acts to reduce ("spoil") the cavity finesse. This leads to nonlinear distortion of the observed molecular line shapes, making a quantitative measurement difficult. Another point to consider is that the cavity must be kept in resonance with the probe beam when the wavelength is tuned. A feedback loop is often used, which adjusts cavity length to track the changes in probe wavelength.[44] The rate of this electromechanical adjustment is much too slow to keep up with the laser tuning rate normally used for sensitive spectroscopy (more on this in section 4.3). Another form of cavity-enhanced spectroscopy is CRDS.[45–48]

An interesting, and remarkably simple, method to increase effective path length through a gas sample has recently been demonstrated by Tranchart et al.[49] It involves the use of a broadband integrating sphere whose inside walls diffuse light rather than reflect it. Effective path length for the probe beam inside the sphere is then given by Equation (12):

$$L_{\text{eff}} = \frac{4R}{3(1-\rho)} \tag{12}$$

Here R is the sphere radius, and ρ the diffuse reflection coefficient. Highly reflective walls ($\rho \to 1$) make it possible to obtain several meters of effective path length from

For references see page 1977

a sphere as small as 10 cm in diameter. This method does not require sophisticated alignment of the probe beam into the sphere, but has the disadvantage of low detected power that is proportional to the ratio of the detector active area to the inside surface area of the sphere.

4.2 Balanced and Balanced-ratiometric Detection

Laser intensity noise and drift may limit the sensitivity with which absorption signals are measured. This is particularly true for gas lasers, or externally pumped solid-state ring lasers, where output power fluctuations induced by acoustic vibration and variations in pump power can exceed 1% full scale. Balanced detection may be used to recover small absorption signals in this situation. Noise detected in an equal-intensity replica of the probe beam, such as that created by a variable-ratio beamsplitter, is subtracted from noise detected in the probe beam, thus leaving only the uncompensated weak absorption signals of interest. A variable-ratio beamsplitter can be made by placing a polarization rotator (a half-wave plate) in series with a polarizing beamsplitter cube, as shown in Figure 11.

With the input polarization rotated about 45°, the beams emerging from the beamsplitter cube carry equal amounts of power P, and power noise ΔP. In the absence of absorption, the photo-currents generated by the (identical) signal and reference detectors can be subtracted to cancel each other exactly. If one of the beams is attenuated due to small absorption a, by a gas, for example, the balance of photo-currents is disturbed, and a signal is seen at the output of the amplifier (Equation 13):

$$V_{out} = R(I_{ref} - I_{sig}) = aRSP + aRS\Delta P \qquad (13)$$

Here R is feedback resistance, and S is the detector element response, in amperes per watt. The second term constitutes noise, and the corresponding signal-to-noise ratio is $P/\Delta P$, independent of absorption a and limited basically by the quality of the probe beam. With the use of a single detector (no balancing), the signal-to-noise ratio would be a mere $aP/\Delta P$, i.e. absorption on the order of $a_{min} = \Delta P/P$ would be indistinguishable from noise. In practice, adjustment of the beam splitting ratio ("zeroing") is necessary to compensate for unequal response of the signal and reference detectors and difference in optical transmission of the signal and reference arms. Moreover, detectors must be sufficiently quiet to resolve fluctuations in probe power, and have equal delay times.

An advanced implementation of this method, proposed by Hobbs[50] and known as balanced ratiometric detection (BRD), uses circuitry to compute a log ratio of photo-currents, rather than their difference, and to cancel noise currents at the same time. The analog divider, whose simplified schematic is shown in Figure 12, uses logarithmic conformance and tight symmetry of base-emitter curves of a matched transistor pair. The summing junction X is held at ground by an error amplifier A_1 whose output is integrated and applied to the base of transistor Q_2. When currents at the summing junction are balanced, the output of A_1 is zero, and the output of A_2 is given by Equation (14):

$$V_{out} = \left(\frac{R_1 + R_2}{R_1}\right)\frac{k_B T}{e}\ln\left(\frac{I_{ref}}{I_{sig}} - 1\right) \qquad (14)$$

Here k_B is the Boltzmann's constant, T the absolute temperature of the matched transistor pair Q_1Q_2, and e

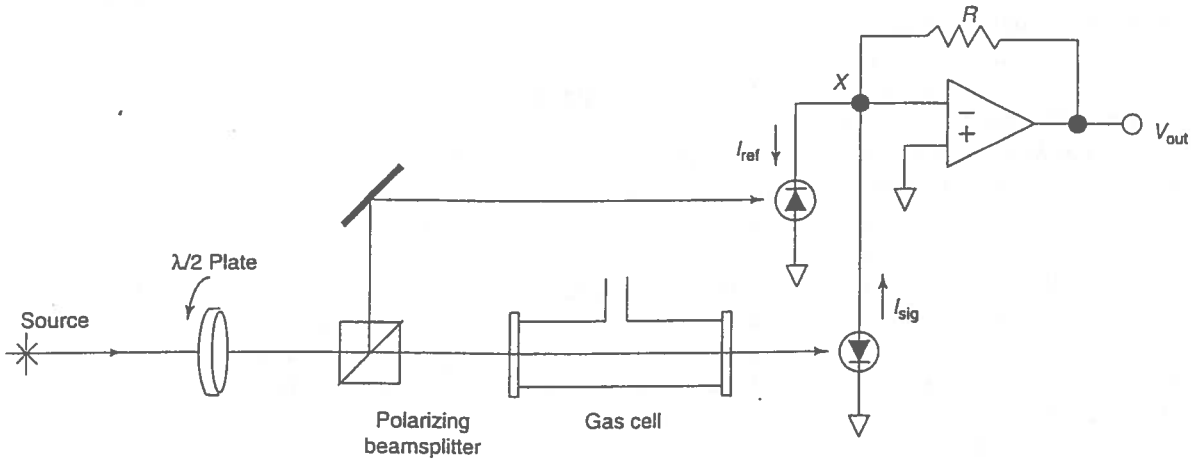

Figure 11 In the simple balanced detection method, a variable-ratio beamsplitter (a combination of a half-wave plate and a polarizing beamsplitter) is used to send nearly equal amounts of optical power to the signal and reference detectors, bringing V_{out} to zero. The balance at the current-summing junction X is maintained despite the laser amplitude noise, since the generated noise photo-currents are of opposite sign and nearly equal magnitude. An imbalance of photo-currents due to absorption in the signal beam results in a nonzero output.

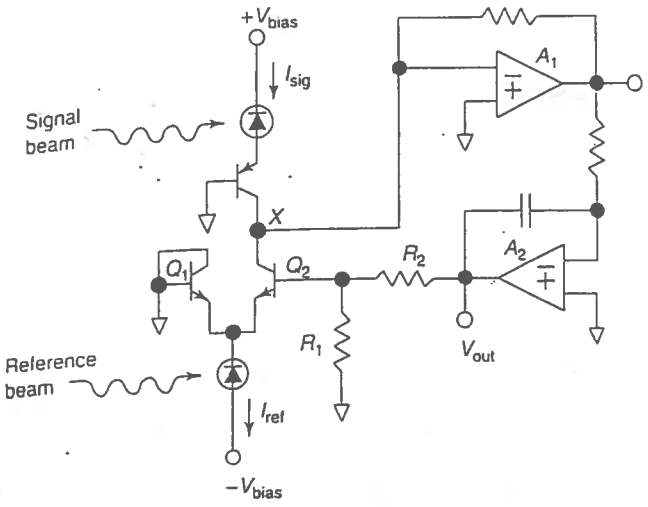

Figure 12 Circuit diagram of a balanced ratiometric detector. When currents at the summing junction X are balanced, the output of the error amplifier A_1 is zero, and the output of the integrator A_2 is proportional to $\ln(I_{ref}/I_{sig} - 1)$. A nearly perfect cancellation of noise photo-currents is achieved when $I_{ref} \approx 2I_{sig}$.

the electron charge. This scheme provides nearly perfect cancellation of noise currents when the reference beam carries roughly twice the power of the signal beam. The signal-to-noise ratio is thus increased well beyond the $P/\Delta P$ limit of the simple balancing scheme described above.

Since the signal versus reference current balancing is performed by means of electronic feedback, no physical adjustment of the beam splitting ratio is necessary. The BRD differential response to absorption signals is nonlinear, however, in that it depends on the ratio of the signal and reference currents which changes when the signal beam is partially absorbed. It also depends on temperature in the same way the transistor base-emitter voltage does, and additional compensation circuitry is needed to produce a useful output voltage V_{out}. Nevertheless, detection sensitivities presently achieved with BRD are quite stunning. Noise-equivalent absorbances as low as 2×10^{-7} Hz$^{-1/2}$ have been demonstrated by Allen et al.,[15] close to the limit imposed by the laser shot noise.

4.3 Frequency and Wavelength Modulation Spectroscopy

The ability of a diode laser to change its emission wavelength with injection current, and to do so very rapidly, is one of the reasons why the diode laser has been so effective in spectroscopic applications. The wavelength change is driven by two effects. Current-induced heating of the semiconductor junction leads to change in optical length of the laser cavity and red-shifts the laser's broad gain curve; this constitutes "coarse" tuning. The current also controls the carrier density which in turn affects the cavity refractive index; this "fine" tuning mechanism is normally at least ten times less pronounced at low frequencies, but becomes dominant at high frequencies (>1 MHz). The tuning response thus depends on the modulation rate and ranges from 2–3 GHz mA^{-1} at low frequencies to under 300 MHz mA^{-1} at high frequencies. FM is always accompanied by amplitude modulation, as the injection current also controls the laser output power (Equation 15):

$$E(t) = A\{1 + m\cos(\Omega t)\}\sin\{wt + \beta\cos(\Omega t + \Phi)\} \quad (15)$$

Here $E(t)$ is the laser electric field, $w = 2\pi c/\lambda$ the laser frequency, and Ω the modulation frequency. By analogy with radio communication, w is the "carrier" frequency. The quantities m and β are the amplitude and FM indices, respectively, and Φ is the generally nonzero phase shift. Sine-wave modulation of the diode laser has the effect of creating multiple side bands in its otherwise nearly monochromatic emission spectrum. Each side band is separated from the carrier by an integer multiple of the modulation frequency Ω, and its relative intensity depends on β.[51]

In *FM spectroscopy*, for example, Ω significantly exceeds the laser linewidth that is typically several tens of megahertz (see Table 2), and m, β are both small, so that only the two first-order side bands, $w + \Omega$ and $w - \Omega$, have appreciable magnitude. After uniform attenuation, such as that encountered in nonresonant optical systems or media (e.g. imaging optics or vacuum), the side bands add up coherently with the carrier and balance each other to produce a beam of nearly constant intensity, A^2. If the attenuation strongly depends on frequency, however, as is the case with most gases, one of the side bands may become unbalanced and lead to the appearance of multiple harmonics of Ω in the detected laser intensity. The strength of absorption determines the magnitude of these harmonics, which may be measured separately and with high noise immunity, by using a lock-in amplifier for example. This is usually done while the laser carrier frequency w is scanned in the vicinity of the absorption line of interest.

This detection technique was first applied by Bjorklund to a CW dye laser.[52] It proved extremely powerful and is widely used in diode laser spectroscopy today, sometimes in modified form such as TTFM,[53] or amplitude modulated phase modulation (AMPM) spectroscopy.[54]

Wavelength modulation (WM) is really another form of FM spectroscopy, in which case the modulation frequency Ω is smaller than the laser linewidth, and the modulation indices m and β are both large.[55] The aforementioned side bands are then present to a very high order and,

For references see page 1977

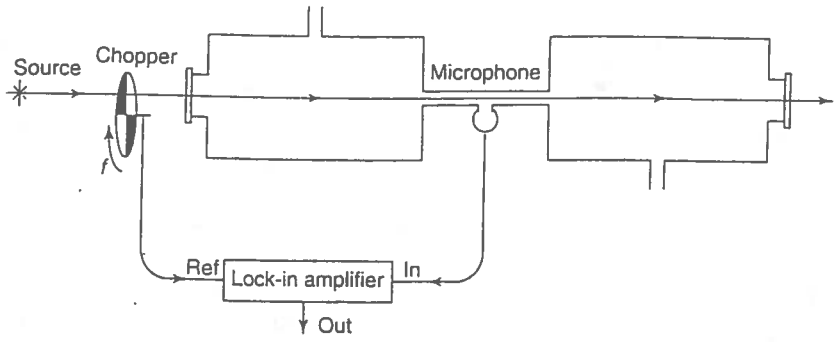

Figure 13 Simplified schematic of an opto-acoustic trace-gas detection system using a resonant acoustic cell. The beam is chopped at a frequency f, and a synchronous acoustic signal is detected by a microphone and a lock-in amplifier. Laser WM on and off the gas absorption line can produce an acoustic signal in much the same way as a chopped beam that is tuned to the line center.

by virtue of their small separation from each other, merge into a continuous spectrum. The detection is again performed at the first, second, or higher harmonics of Ω as the laser carrier frequency w is scanned in the vicinity of a gas absorption line. WM spectroscopy dominates applications that rely on relatively low-speed detectors, and its sensitivity is limited by the laser amplitude $1/f$ noise.

4.4 Opto-acoustic Detection

Optical power absorbed by a gas from the probe beam leads to local heating of the gas and inevitably generates a local pressure differential. The pressure differential can, in principle, be detected as an acoustic pulse, some distance away from the source in any direction. A train of acoustic pulses at a known frequency (a "tone"), such as that produced in a gas by a chopped beam, for example, can be detected using a microphone and a lock-in amplifier (see Figure 13). Since power absorbed from the probe beam depends on wavelength, a change in the intensity of the acoustic wave will result as the laser wavelength is tuned. Spectroscopy based on this principle is called *opto-acoustic spectroscopy* (*OAS*), or *photo-acoustic spectroscopy* (*PAS*). It has one important advantage: in the absence of an absorbing gas there is no acoustic signal at all. External acoustic noise is unimportant, as it has random phase relative to the chopper and is therefore filtered away effectively by the lock-in amplifier. At some level of scrutiny, however, one might find interfering synchronous acoustic signals, such as those generated by the slightly absorbing windows of the sample cell, etc.

Since the opto-acoustic signal is proportional to beam intensity, the method has been used primarily with high-power infrared lasers, such as CO_2 and CO.[56] Low-power diode lasers are now being used as well, although gas cells are often built as acoustic resonators in order to increase the observed signal.[57] Surprisingly, the WM capabilities of diode lasers have found an elegant use in OAS – periodic tuning of the laser beam on and off the line resonance is also a good way to generate an acoustic wave. The theory for WM opto-acoustic signal generation involves coupled heat transfer and the Navier–Stokes equations[58] and is beyond the scope of this review.

5 EXAMPLES OF TRACE-GAS SENSORS

Here we will describe practical embodiments of the three types of laser spectroscopic sensors described in section 3. These are sensors based on NIR semiconductor lasers, lead-salt diode lasers, and diode laser frequency conversion. We have selected one instrument in each category as an example. These instruments have either stimulated a development of a broad range of similar sensors and related measurement techniques, or are an example of how multiple elements of the developed sensor technology function together in a complete spectroscopic instrument.

5.1 Gas Sensors Based on Near-infrared Diode Laser Overtone Spectroscopy

Intense development of gas sensors based on visible and NIR semiconductor lasers has been reported by groups in the USA, Europe, and Japan.[42,50] Applications in which these sensors find increasing use are combustion diagnostics, landfill emissions monitoring, natural-gas leak detection, optical sensing of flows, and industrial process control. One of the first applications of a NIR diode laser to gas detection was reported in 1992 by Uehara and Tai.[16] Figure 14 shows a schematic diagram of spectrometer built for the purpose of detecting methane in ambient air; it uses the same transmitter design in two remote detection schemes. The transmitter employs a 1.665-μm InGaAsP DFB diode laser developed

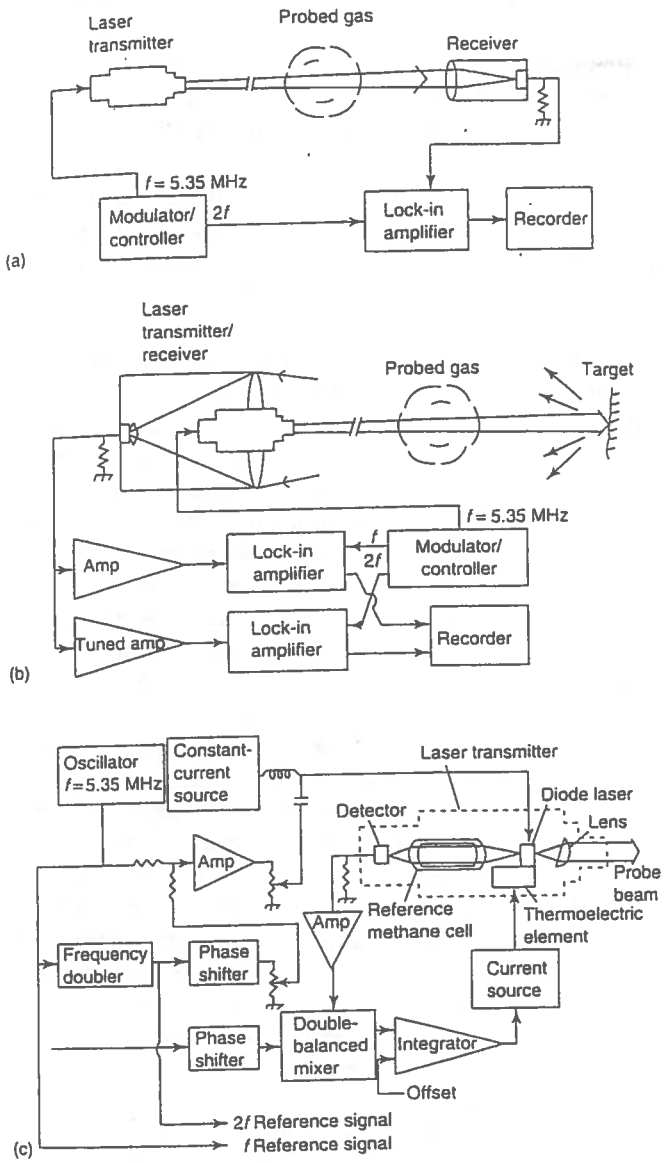

Figure 14 Diode laser methane sensor developed by Uehara and Tai,[16] in two remote detection schemes: transmission (a) and reflection (b). Schematics of the laser transmitter and its modulation controller are shown in (c). The transmitter housing is 4 cm in diameter.

specifically for the detection of methane in the $2\nu_3$ stretch vibration overtone band.

Laser emission in this instrument was available from both front and rear facets of the laser chip, and was detected using InGaAs pin photodiodes. The backward beam was used to dither-lock the laser wavelength to the center of the Q(6) line of methane in a reference cell. The 3-cm-long pyrex cell contained 200 torr of methane mixed with 560 torr of air. The cell windows functioned as lenses: one collimated the laser output while the other focused it on to a reference detector. The laser injection current was modulated at a rate of $f = 5.35$ MHz and the output of the reference detector was processed by a double-balanced mixer to recover the amplitude of the first harmonic ($1f$) of the modulation frequency. Due to AM–FM cross-talk in the diode laser, the amplitude is nonzero even in the absence of absorption, therefore offset cancellation was used to produce a suitable error signal. The error signal crosses zero when the laser frequency is scanned across the center of the absorption line, and therefore can be used, upon integration, as feedback to control the laser temperature. Such a simple locking scheme was reported to stabilize the center wavelength to within 10 MHz of the absorption line. After frequency stabilization was obtained, a small-amplitude second harmonic ($2f$) signal was added to the laser injection current to compensate the residual $2f$ signal amplitude in the detected *forward* laser beam in the absence of absorption. Absorption caused by the presence of methane in the signal beam path was then registered as a positive $2f$ amplitude.

Figure 15 shows an example of instrument output in the transmission scheme, in which the second harmonic amplitude alone was recorded. The signal was caused by a 100-ppm mixture of methane in air in a 50-cm-long cell. The mixture was introduced into the cell and purged subsequently with nitrogen, resulting in zero output after two minutes. The signal-to-noise ratio in the trace corresponds to a minimum detectable CH_4 column density of 0.3 ppm m, achieved using a signal averaging time of 1.3 s.

In the reflection detection scheme, the registered amplitude of the second harmonic depends not only on absorption, but on the range to the scattering target and on the target reflectance (wooden boards and concrete blocks were used). The amplitude of the first harmonic is directly proportional to the received optical power;

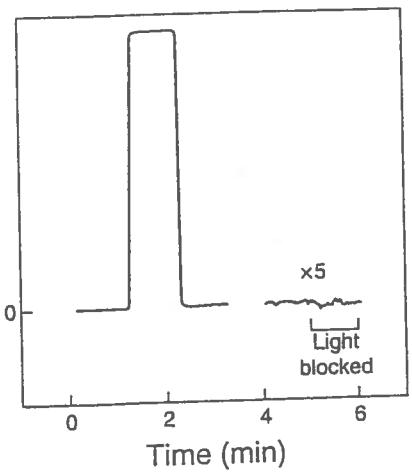

Figure 15 A $2f$ signal derived from a methane column density of 50 ppm m, lock-in-detected in the transmission scheme.[16] An inset on the right shows a ×5 magnified noise. No background shift is observed when the laser beam is blocked.

For references see page 1977

quantitative detection was thus performed by computing a ratio of the $2f$ and $1f$ amplitudes. The corresponding detection sensitivity was 50 ppm m. Although higher modulation frequencies are advantageous for noise reduction, caution must be exercised when they are used in the reflection scheme. When the beam path length from transmitter to receiver changes, the detected phases of the first and second harmonics also change. For a modulation frequency of 5.35 MHz, for example, a 3.5-m change in distance to target results in a 90° phase shift in the second-harmonic signal. The phase shift must be tracked and compensated in order to maintain maximum signal intensity.[51,59–63]

5.2 Tuneable Mid-infrared Diode Laser Absorption Spectrometer

In the area of MIR spectroscopy, the airborne tuneable laser absorption spectrometer (ATLAS) developed by Podolske and Loewenstein[19] is an example of a self-contained field instrument. It was developed for in situ measurement of nitrous oxide and carbon monoxide in the lower stratosphere from an ER-2 high-altitude aircraft. Optical layout of the instrument is shown in Figure 16. A pressure-regulated liquid nitrogen Dewar housed two different lead-salt lasers: one operating at 2169.2 cm^{-1} for the detection of carbon monoxide, and another at 1270.2 cm^{-1} for the detection of nitrous oxide. After collimation by an off-axis parabolic mirror, the beam passed through an adjustable iris and the diagnostics section, and was then partitioned into three beams (sample, reference, and zero) by organic pellicle beamsplitters. These have the advantage of negligible thickness, hence beam displacement, and small, 5–10%, amount of deflected light, so that most of optical power remained in the sample beam. All three beams were measured by identical detectors. InAs detectors were used for the measurement of carbon monoxide at 4.7 μm, and HgCdTe detectors were used for the measurement of NO at 8 μm.

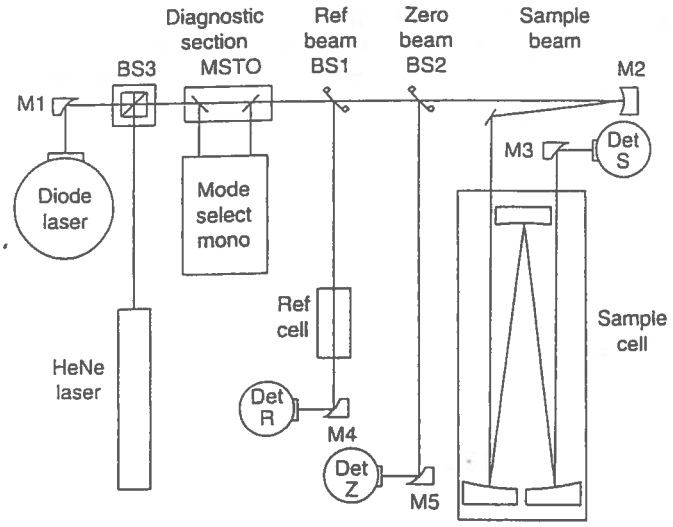

Figure 16 Optical layout of ATLAS, by Podolske and Loewenstein.[26] The sample, reference, and zero beams are detected by detector S, R, and Z, respectively. The zero beam has the same optical path length as the sample beam external to the White cell. A bidirectional alignment beam is formed by a beamsplitter BS3, illuminated by a HeNe laser. Mode selecting monochromator and mode-selecting transfer optics are optional.

The instrument employed a noticeably complex laser current modulation and control scheme. Up to eight signals were superimposed to determine the instantaneous laser wavelength. Two of them were generated by an on-board computer for coarse and fine adjustment of the center wavelength. An adjustable amplitude, 2-kHz sine wave was added to perform WM spectroscopy. The $1f$ feedback signal derived from the reference channel was also added for locking of the laser wavelength to the center of a chosen absorption line (R(6) for carbon monoxide, or P(17) for nitrous oxide). A 12.8-kHz triangle wave dither was also added to suppress the effective magnitude of optical interference fringes. Another signal, a 125-Hz triangle wave was used to perform frequency scans for display purposes during instrument set-up. For the measurement of dark detector output, each period of the waveform was preceded by a 125 μs pulse that gated off the laser injection current. Each gate pulse was immediately followed by another, adjustable compensation pulse that provided heating of the laser junction that would have occurred in the absence of the gate pulse. The use of this compensation diminished the frequency drift associated with thermal recovery of the laser junction after each gate pulse.

In addition to optics, the ATLAS included a calibration and gas flow system (see Figure 17). The gas flow system routed and conditioned the flow of both the reference gas

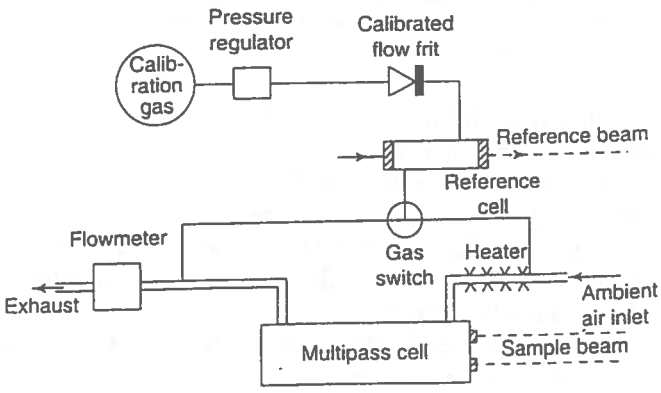

Figure 17 Diagram of the calibration and gas flow system of the ATLAS instrument.[26]

(100 ppm CO in nitrogen or 1000 ppm N_2O in nitrogen) and the sample. Air was sampled from outside the aircraft boundary layer by means of a narrow inlet tube, into which the air was propelled by ram pressure. The air then passed through a multipass cell with a residence time of approximately 1 s. Gas pressure and temperature inside the cell were maintained approximately equal that of the reference cell. Pressure equalization was accomplished by a feedback-controlled flow of the reference gas through a frit, rather than by making it a static specimen. Gas temperatures were made equal by heating of the incoming air to 25 °C; this also prevented temperature-induced alignment drift of the cell mirrors. For airborne measurements of nitrous oxide, whose typical abundance in air is approximately 300 ppb, the uncertainty of ±10% was estimated for ATLAS when using a signal averaging time of 1 s.

Apart from the systems described, the ATLAS had several electronic subsystems: laser control, analog signal processing, data acquisition, computer, and the pressure and temperature control. To fully appreciate the complexity of an actual instrument designed for field applications it is helpful to consult Fried et al.[24,64] and Nelson et al.[63]

5.3 Gas Sensors Based on Difference Frequency Generation Absorption Spectroscopy

As described in section 3.4, difference frequency mixing of near infrared CW or pulsed laser sources is another convenient technique to access the molecular "fingerprint" region. Until recently, DFG sensors used discrete optical components to generate microwatt-level CW radiation.[31,65–68] More recently, the technologies developed for optical telecommunications – optical fiber, and rare-earth-doped fiber amplifiers – have been used in DFG sensors. This approach has improved the robustness and reliability, since it ensures permanent alignment of DFG pump channels without an increase in device complexity and cost. Lancaster et al.[67] built a portable sensor that is tuneable from 3.25 to 4.4 μm (see Figure 7).

A 20-mW ECDL with a tuning range of 814–870 nm, and an Yb-doped fiber amplifier seeded by a 1083-nm DBR were mixed in a multi-grating, temperature-controlled PPLN crystal. A 7.2-m long fiber amplifier, pumped by a 2-W diode laser at 975 nm, produced 590 mW output power when seeded with 12 mW. All amplifier components were packaged into a 9 × 11 × 2 cm^3 housing.

The pump wavelengths were combined by a low-loss fiber directional coupler. An $f = 1$ cm Achromat lens was used for imaging the fiber output into the PPLN crystal. A 19-mm long, 0.5-mm thick crystal was used, with broadband antireflection coatings applied to both end faces. The crystal had 8 domain grating periods, from 22.4 to 23.1 μm in 0.1 μm increments, and was temperature-controlled in the 10–85 °C range. The DFG radiation is collimated by an $f = 5$ cm CaF_2 lens and the residual pump light was blocked by a germanium filter. The radiation is either focused directly on a Peltier-cooled HgCdTe detector or aligned through a compact multipass cell with an effective path length from 18 to 100 m. The data acquisition system used was similar to the one described in Topfer[31] and Lancaster,[70] and consists of a compact 16-bit analog-to-digital converter card and a notebook computer. Detector voltage was sampled at a rate of 100 kHz and processed using a 9 kHz digital low-pass filter.

Coarse frequency tuning of the Littman-cavity ECDL (Figure 4) was performed by rotation of its tuning mirror with respect to the diffraction grating. The advantage of this configuration is a beam direction and a point of origin that are independent of wavelength; this allows stable coupling into an optical fiber. Fine tuning and repetitive frequency scans of up to 25 GHz were accomplished by linear current modulation of the seed DBR diode laser at a rate of 200 Hz. The instrument linewidth of 42 ± 5 MHz was measured indirectly by spectroscopy of methane at low pressure. Figure 18 shows the individual direct absorption spectra of six species of interest for trace-gas detection that are within the 3.25–4.4 μm tuning range of the sensor, including CO_2, N_2O, H_2CO, HCl, NO_2 and CH_4. These spectra were taken at reduced pressure (88 torr) in a multipass cell using either calibrated gas mixtures or room air. Fitted Lorentzian line shapes were used to determine gas concentrations. Stability of instrument performance was assessed by monitoring of a methane line at 3028.751 cm^{-1} for an extended time period. In this experiment a calibrated 1772.7 ± 1 ppb mixture of CH_4 in air was continuously flown through the multipass cell at a pressure of 88 torr. Observed standard deviation of the measurement was 0.8% (15 ppb).

The instrument occupies a 45 × 45 cm^2 optical breadboard mounted in a reinforced plastic suitcase for portability and weighing 25 kg. Total power consumption is approximately 60 W. To provide a continuous gas flow through the multipass cell at a controlled pressure, a two-stage diaphragm pump was used in series with a pressure flow controller. A capacitive manometer was used to measure the gas pressure just prior to the multipass cell. For the measurement of reactive gases such as H_2CO, HCl and NO_2, the gas handling system was maintained at 40 °C.

6 CONCLUSION

Spectroscopic sources for trace-gas monitoring, based on diode lasers, find increasing use in both established

For references see page 1977

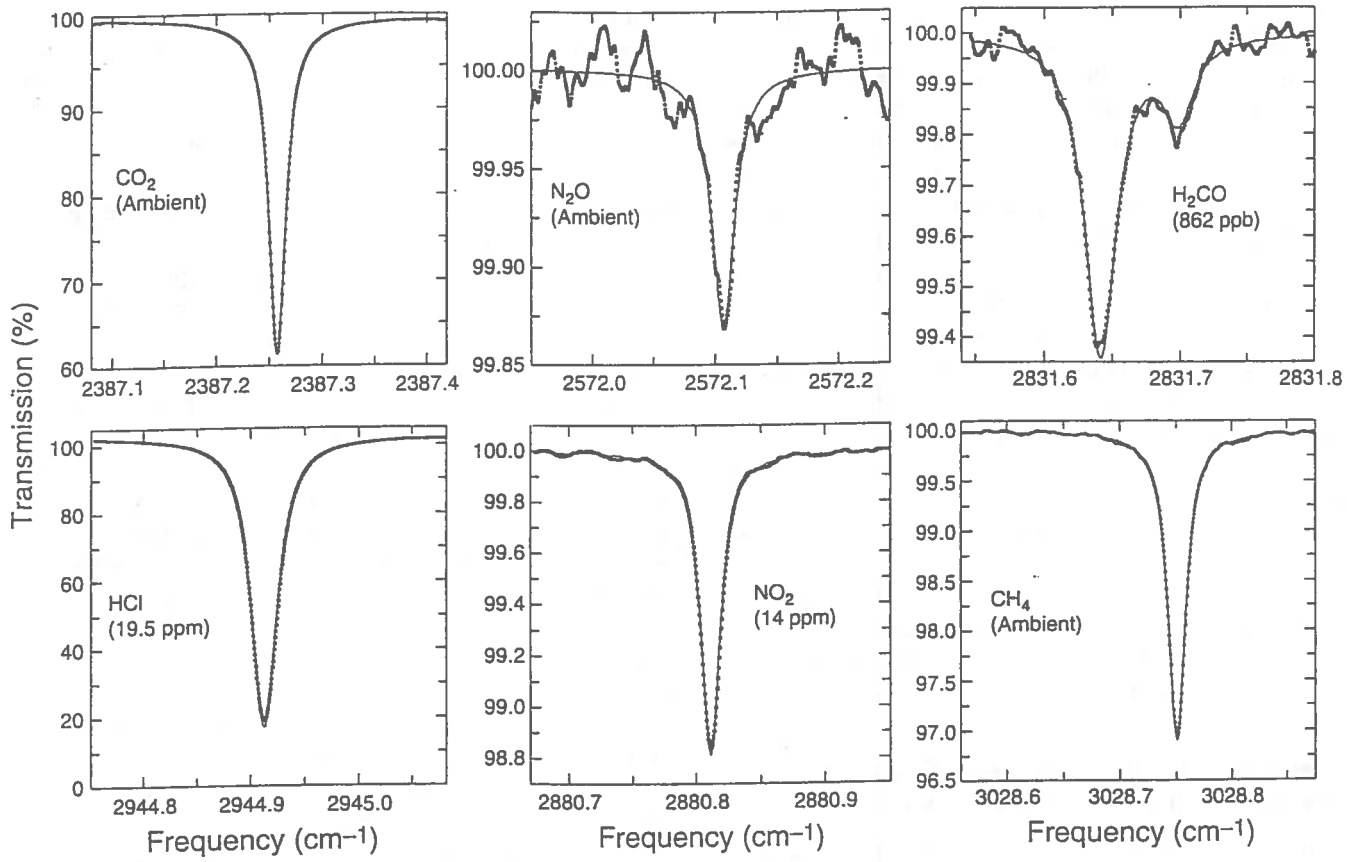

Figure 18 Detected absorption lines of several atmospheric trace gases.[69]

and new fields, including air-quality control; atmospheric chemistry; industrial, traffic, and agricultural emissions; chemical analysis and process control; and medical diagnostics. The moderate cost, compact gas sensor using all-solid-state technology is capable of highly sensitive, selective detection and real-time analysis of a large number of gas species by means of absorption spectroscopy in the overtone and fundamental spectral regions. Reductions in cost and complexity, coupled with improved reliability and ease of operation, are now made as a result of the availability of several novel technologies developed by the telecommunications and computer industries that are equally applicable and useful in state-of-the-art gas sensors.

ACKNOWLEDGMENTS

The authors gratefully acknowledge stimulating input by a number of present and previous coworkers, graduate students and collaborators. This chapter also benefited from helpful suggestions and critical comments by Mark Allen of Physical Sciences, Inc. (Boston) and Adam Holyoake (John Wiley & Sons, Inc.).

ABBREVIATIONS AND ACRONYMS

AMPM	Amplitude Modulated Phase Modulation
ATLAS	Airborne Tuneable Laser Absorption Spectrometer
BRD	Balanced Ratiometric Detection
CRDS	Cavity Ring Down Spectroscopy
CW	Continuous Wave
DBR	Distributed Bragg Reflector
DFB	Distributed Feedback
DFG	Difference-frequency Generation
ECDL	External-cavity Diode Laser
FM	Frequency Modulation
KTP	Potassium Titanyl Phosphate
MDC	Minimal Detectable Concentration
MIR	Mid-infrared
NIR	Near-infrared
OAS	Opto-acoustic Spectroscopy.
PAS	Photo-acoustic Spectroscopy
TTFM	Two-tone Frequency Modulation
WM	Wavelength Modulation

List of selected abbreviations appears in Volume 15

RELATED ARTICLES

Environment: Trace Gas Monitoring **(Volume 3)**
Environmental Trace Species Monitoring: Introduction • Differential Optical Absorption Spectroscopy, Air Monitoring by • Fourier Transform Infrared Spectrometry in Atmospheric and Trace Gas Analysis • Infrared LIDAR Applications in Atmospheric Monitoring • Laser Absorption Spectroscopy, Air Monitoring by Tunable Mid-infrared Diode • Laser-based Combustion Diagnostics • Photoacoustic Spectroscopy in Trace Gas Monitoring

REFERENCES

1. M.W. Sigrist (ed.), *Air Monitoring by Spectroscopic Techniques*, Chemical Analysis, John Wiley & Sons, Inc., New York, Vol. 27, 1994.
2. M.W. Sigrist, 'Air Monitoring, Optical Spectroscopic Methods', in *Encyclopedia of Environmental Analysis and Remediation*, ed. R.A. Meyers, John Wiley & Sons. Inc., New York, 84–117, 1998.
3. A.G. Maki, J.S. Wells, *Wavenumber Calibration Tables from Heterodyne Frequency Measurements*, Spec. Publ. 821 (Natl. Inst. Stand. Technol., Gaithersburg, MD). 1991.
4. L.S. Rothman, R.R. Gamache, A. Goldman, L.R. Brown, R.A. Toth, H.M. Pickett, R.L. Poynter, J.-M. Flaud, C. Camy-Peyret, A. Barbe, N. Husson, C.P. Rinsland, M.A.H. Smith, 'The HITRAN database: 1986 edition', *Appl. Opt.*, **26**, 4058 (1987).
5. GEISA database, Laboratoire de Meteorologie Dynamique du CNRS, Ecole Polytechnique, F-91128 Palaiseau Cedex, France.
6. R.M. Mihalcea et al., *Appl. Phys. B* – Lasers and Optics, Special Issue, August (1998).
7. D.M. Sonnenfroh, M.G. Allen, *Appl. Opt.*, **36**, 18 (1997).
8. Norsk Elektro Optikk, 'Laser Gas Monitors, Technical Description', Norway, 1996.
9. Southwest Sciences Inc., 'Detection Limits', http://www.iac.net/~dchovde/.
10. Bovar – Western Research, 'Spectrascan: Technical Specifications', Ref. No. 908-0001 Rev. 0.
11. M.G. Allen et al., *Appl. Opt.*, **34**, 18 (1995).
12. M. Feher et al., *Appl. Opt.*, **32**, 12 (1993).
13. J. Humlicek, 'An Efficient Method for Evaluation of the Complex Probability Function: The Voigt Function and its Derivatives', *J. Quant. Spectrosc. Radiat. Transfer*, **21**, 309 (1979).
14. C.E. Wieman, L. Hollberg, 'Using Diode Lasers for Atomic Physics', *Rev. Sci. Instrum.*, **62**, 1 (1991).
15. M.G. Allen, K.L. Carleton, S.J. Davis, W.J. Kessler, C.E. Otis, D.A. Palombo, D.M. Sonnenfroh, 'Ultra Sensitive Dual Beam Absorption and Gain Spectroscopy: Applications for Near-infrared and Visible Diode Laser Sensors', *Appl. Opt.*, **34**, 3240 (1995).
16. K. Uehara, H. Tai. 'Remote Detection of Methane with a 1.66 μm Diode Laser', *Appl. Opt.*, **31**, 809 (1992).
17. H. Tai, K. Yamamoto, M. Uchida, S. Osawa, K. Uehara, 'Long Distance Simultaneous Detection of Methane and Acetylene by Using Diode Lasers Coupled with Optical Fibers', *IEEE Photon. Technol. Lett.*, **4**, 804 (1992).
18. A.T. Schremer, C.L. Tang, *IEEE Photon. Technol. Lett.*, **2**, 3 (1990).
19. D.B. Oh, D.C. Hovde, 'Wavelength-modulation Detection of Acetylene with Near-infrared External Cavity Diode Laser', *Appl. Opt.*, **34**, 7002 (1995).
20. Z. Feit, D. Kostyk, R.J. Woods, P. Mak, 'Molecular Beam Epitaxy Grown PbEuSeTe Buried-heterostructure Lasers with Continuous Wave Operation @ 195 K', *Appl. Phys. Lett.*, **57**, 2891 (1990).
21. J. Reid, M. El-Sherbiny, B.K. Garside, E.A. Ballik, 'Sensitivity Limits of a Tunable Diode Laser Spectrometer with Application to the Detection of NO_2 @ the 100 ppt. Level', *Appl. Opt.*, **19**, 3349 (1980).
22. H.I. Schiff, D.R. Karecki, G.W. Harris, D.R. Hastie, G.I. Mackay, 'A Tunable Diode Laser System for Aircraft Measurements of Trace Gas', *J. Geophys. Res.*, **95**, 10 147 (1990).
23. M. Kohl, D. Wohrle, et al., 'Delayed Observation of Laser Induced Fluorescence for Imaging of Tumors', *Appl. Phys. B*, **57**, 131 (1993).
24. A. Fried, S. McKeen, S. Sewell, J. Harder, B. Henry, P. Golden, 'Photochemistry of Formaldehyde During the 1993 Tropospheric OH Photochemistry Experiment', *J. Geophys. Res.*, **102**, 6283 (1997).
25. C.R. Webster, R.D. May, 'Simultaneous In Situ Measurements and Diurnal Variations of NO, NO_2, O_3, jNO_2, CH_4, H_2O, and CO_2 in the 40–26-km Region Using an Open Path Tunable Diode Laser Spectrometer', *J. Geophys. Res.*, **92**, 11 931 (1987).
26. J. Podolske, M. Loewenstein, 'Airborne Tunable Diode Laser Spectrometer for Trace Gas Measurement in the Lower Stratosphere', *Appl. Opt.*, **32**, 5324 (1993).
27. A.S. Pine, *J. Opt. Soc. Am.*, **64**, 1683 (1974).
28. U. Simon, C.E. Miller, C.C. Bradley, R.G. Hulet, R.F. Curl, F.K. Tittel, 'Difference Frequency Generation in $AgGaS_2$ by Use of Single Mode Diode Laser Pump Sources', *Opt. Lett.*, **18**, 1062 (1993).
29. G. Rosenman, Kh. Garb, A. Skliar, M. Oron, D. Eger, M. Katz, 'Domain Broadening in Quasi-phase Matched Nonlinear Optical Devices', *Appl. Phys. Lett.*, **73**, 865 (1998).
30. L.E. Myers, W.R. Bosenberg, 'Periodically Poled Lithium Niobate and Quasi-phase-matched Optical Parametric Oscillators', *IEEE J. Quant. Electron.*, **33**, 1663 (1997).
31. T. Topfer, K.P. Petrov, Y. Mine, D. Jundt, R.F. Curl, F.K. Tittel, 'Room Temperature Mid-infrared Laser Sensor for Trace Gas Detection', *Appl. Opt.*, **36**, 8042 (1997).

List of selected abbreviations appears in Volume 15

32. G.D. Boyd, D.A. Kleinman, *J. Appl. Phys.*, **39**, 3597 (1968).
33. T.B. Chu, Q. Broyer, *J. Phys.*, **46**, 523 (1985).
34. L. Goldberg, W.K. Burns, R.W. McElhanon, 'Difference Frequency Generation of Tunable Mid-infrared Radiation in Bulk Periodically Poled $LiNbO_3$', *Opt. Lett.*, **20**, 1280 (1995).
35. M.L. Bortz, M.A. Arbore, M.M. Fejer, 'Quasi-phase Matched Optical Parametric Amplification and Oscillation in Periodically Poled $LiNbO_3$ Waveguides', *Opt. Lett.*, **20**, 49 (1994).
36. J. Webjörn, F. Laurell, G. Arvidsson, *J. Lightwave Technol.*, **7**, 1597 (1989).
37. C.E. Rice, *J. Solid State Chem.*, **64**, 188 (1986).
38. M.H. Chou, M.A. Arbore, M.M. Fejer, 'Adiabatically Tapered Periodic Segmentation of Channel Waveguides for Node-size Transformation and Fundamental Mode Excitation', *Opt. Lett.*, **21**, 794 (1996).
39. M.H. Chou, J. Hauden, M.A. Arbore, M.M. Fejer, '1.5-μm Band Wavelength Conversion Based on Difference Frequency Generation in $LiNbO_3$ Waveguides with Integrated Coupling Structures', *Opt. Lett.*, **23**, 1004 (1998).
40. K.P. Petrov, A.T. Ryan, T.L. Patterson, L. Huang, S.J. Field, D.J. Bamford, 'Mid-infrared Spectroscopic Detection of Trace Gases Using Guided-wave-difference-frequency Generation', *Appl. Phys. B*, **67**, 357 (1998).
41. W.B. Grant, R.H. Kagann, W.A. McClenny, *J. Air Waste Manage. Assoc.*, **42**, 18 (1992).
42. J.B. McManus, P.L. Kebabian, M.S. Zahniser, 'Astigmatic Mirror Multipass Absorption Cells for Long-path Length Spectroscopy', *Appl. Opt.*, **34**, 3336 (1995).
43. K. Nakagawa, T. Katsuda, A.S. Shelkovnikov, M. de Labachelerie, M. Ohtsu, 'Highly Sensitive Detection of Molecular Absorption Using a High Finesse Optical Cavity', *Opt. Commun.*, **107**, 369 (1994).
44. K.P. Petrov, S. Waltman, U. Simon, R.F. Curl, F.K. Tittel, E.J. Dlugokencky, L. Hollberg, 'Detection of Methane in Air Using Diode-laser Pumped Difference Frequency Generation Near 3.2 μm', *Appl. Phys. B*, **61**, 553 (1995).
45. G. Meijer, M.G.H. Boogaarts, R.T. Jongma, D.H. Parker, A.M. Wodtke, 'Coherent Cavity Ring Down Spectroscopy', *Chem. Phys. Lett.*, **217**, 112 (1994).
46. G. Meijer, M.G.H. Boogaarts, R.T. Jongma, D.H. Parker, A.M. Wodtke, 'Cavity Enhanced Absorption and Cavity Enhanced Magnetic Rotation Spectroscopy', *Rev. Sci. Instrum.*, **69**, 3763 (1998).
47. J.J. Scherer, J.B. Paul, C.P. Collier, A. O'Keefe, D.J. Rakestra, R.J. Saykally, *Spectroscopy*, **11**, 46 (1996).
48. J.J. Scherer, J.B. Paul, C.P. Collier, A. O'Keefe, D.J. Rakestra, R.J. Saykally, *Spectroscopy*, **14**, 24 (1999).
49. S. Tranchart, I.H. Bachir, J.-L. Destombes, 'Sensitive Trace Gas Detection with Near Infrared Laser Diodes and an Integrating Sphere', *Appl. Opt.*, **35**, 7070 (1996).
50. P.C.D. Hobbs, IBM Corp, Armonk, N.Y. 'Noise Canceling Circuitry for Optical Systems with Signal Dividing and Combining Means', US Patent No. 5,134,276 (July 28, 1992).
51. P. Werle, 'A Review of Recent Advances in Semiconductor Laser Based Gas Monitors', *Spectrochimica Acta*, Part A (1998).
52. G.C. Bjorklund, 'Frequency-modulation Spectroscopy: A New Method for Measuring Weak Absorption and Dispersions', *Opt. Lett.*, **5**, 15 (1980).
53. D.E. Cooper, T.F. Gallagher, 'Double Frequency Modulation Spectroscopy: High Modulation Frequency with Low-bandwidth Detectors', *Appl. Opt.*, **24**, 1327 (1985).
54. R. Großkloß, P. Kersten, W. Demtröder, 'Sensitive Amplitude- and Phase-modulated Absorption-spectroscopy with a Continuously Tunable Diode Laser', *Appl. Phys. B*, **58**, 137 (1994).
55. F.S. Pavone, M. Inguscio, 'Frequency and Wavelength Modulation Spectroscopies: Comparison of Experimental Methods Using an AlGaAs Diode Laser', *Appl. Phys. B*, **56**, 118 (1993).
56. M.W. Sigrist, S. Bernegger, P.L. Meyer, 'Atmospheric Pollution Monitoring Using CO_2 Laser Photoacoustic Spectroscopy and Other Techniques', *Rev. Sci. Instrum.*, **61**, 1779 (1990).
57. M. Fehér, Y. Jiang, J.P. Maier, A. Miklós, 'Optoaccoustic Trace-gas Monitoring with Near Infrared Diode Lasers', *Appl. Opt.*, **33**, 1655 (1994).
58. A. Miklós, Z. Bozóki, Y. Jiang, M. Fehér, 'Experimental and Theoretical Investigation of Photoacoustic Signal Generation by Wavelength Modulated Diode Lasers', *Appl. Phys. B*, **58**, 483 (1994).
59. M.G. Allen, 'Diode-laser Absorption Sensors for Gas-dynamic and Combustion Flows', *Meas. Sci. Technol.*, **9**, 545 (1998).
60. D.M. Sonnenfroh, W.J. Kessler, J.C. Magill, B.L. Upschulte, M.G. Allen, J.D.W. Barrick, 'In-situ Sensing of Tropospheric Water Vapor Using an Airborne Near Infrared Diode Laser Hygrometer', *Appl. Phys. B*, **67**, 275 (1998).
61. R.M. Mihalcea, M.E. Webber, D.S. Baer, R.K. Hanson, G.S. Feller, W.B. Chapman, 'Diode-laser Absorption Measurements of CO_2, H_2O, N_2O, and NH_3 near 2.0 μm', *Appl. Phys. B*, **67**, 283 (1998).
62. G. Modugno, C. Corsi, M. Gabrysch, F. Marin, M. Inguscio, 'Fundamental Noise Source in a High Sensitivity Two Tone Frequency Modulation Spectrometer and Detection of CO_2 at 1.6 μm and 2 μm', *Appl. Phys. B*, **67**, 289 (1998).
63. D.D. Nelson, M.S. Zahniser, J.B. McManus, C.E. Kolb, J.L. Jimenez, 'A Tunable Diode Laser System for the Remote Sensitive of On-road Vehicle Emissions', *Appl. Phys. B*, **67**, 433 (1998).
64. A. Fried, B. Henry, B. Wert, S. Sewell, J.R. Drummond, 'Laboratory, Ground-based, and Airborne Tunable Diode Laser Systems: Performance Characteristics and Applications in Atmospheric Studies', *Appl. Phys. B*, **67**, 317 (1998).

List of selected abbreviations appears in Volume 15

65. K.P. Petrov, R.F. Curl, F.K. Tittel, 'Compact Laser Difference Frequency Spectrometer for Multi-component Trace Gas Detection', *Appl. Phys. B*, 66, 531 (1998).
66. M. Seiter, D. Keller, M.W. Sigrist, 'Broadly Tunable Difference-frequency Spectrometer for Trace Gas Detection with Nonlinear Critical Phase-matching in $LiNbO_3$', *Appl. Phys. B*, 67, 351 (1998).
67. B. Sumpf, D. Rehle, T. Kelz, H.-D. Kronfeldt, 'A Tunable Diode-laser Spectrometer for the MIR Region Near 7.2 μm Applying Difference Frequency Generation in $AgGaSe_2$', *Appl. Phys. B*, 67, 369 (1998).
68. W. Chen, G. Mouret, D. Boucher, 'Difference-frequency Laser Spectroscopy Detection of Acetylene Trace Constituent', *Appl. Phys. B*, 67, 375 (1998).
69. D.G. Lancaster, D. Richter, F.K. Tittel, Accepted by *Appl. Phys. B*, 459 (1999).
70. D.G. Lancaster, D. Richter, R.F. Curl, F.K. Tittel, 'Real-time Measurements of Trace Gas Using a Compact Difference Frequency Based Sensor Operation at 3.5 μm', *Appl. Phys. B*, 67, 339 (1998).